



# Direct *ab initio* calculation of magnons in altermagnets: Method, spin-space symmetry aspects, and application to MnTe

L. M. Sandratskii <sup>1,2,\*</sup>, K. Carva <sup>1</sup> and V. M. Silkin<sup>2,3,4</sup>

<sup>1</sup>*Faculty of Mathematics and Physics, Charles University, 12116 Prague, Czech Republic*

<sup>2</sup>*Donostia International Physics Center (DIPC), Paseo de Manuel Lardizabal 4, E-20018 San Sebastián, Spain*

<sup>3</sup>*Departamento de Polímeros y Materiales Avanzados: Física, Química y Tecnología, Facultad de Ciencias Químicas, Universidad del País Vasco (UPV-EHU), Apdo. 1072, E-20080 San Sebastián, Spain*

<sup>4</sup>*IKERBASQUE, Basque Foundation for Science, 48011 Bilbao, Spain*



(Received 29 December 2024; accepted 14 May 2025; published 27 May 2025)

We suggest the first method for direct *ab initio* calculation of adiabatic magnons in complex collinear magnets. The method is based on the density-functional-theory (DFT) calculation under two different constraints: one constraint governs the change of the magnetization with respect to the ground state, and the other is the symmetry constraint responsible for the value of the magnon wave vector. The advantages of the suggested method with respect to the usual approach of mapping of the electron system on the Heisenberg Hamiltonian of interacting magnetic moments are discussed. The performance of the method is demonstrated by the application to an altermagnet MnTe. The altermagnetism introduced as a concept in 2022 is at present an area of highly intensive research. The characteristic feature of altermagnets is the spin splitting of the electron states in reciprocal  $\mathbf{k}$  space. Among the discovered properties of the altermagnets is the chirality splitting of the magnons in wave vector  $\mathbf{q}$  space. We suggest an approach to the study of the symmetry aspects of magnon chirality splitting. We show that both the chirality splitting of the magnons and the altermagnetic spin splitting of the electron states, though very different in their physical nature, have identical patterns in the corresponding wave vector spaces. Since the altermagnetism of MnTe is the consequence of the presence of the Te atoms, adequate attention is devoted to the symmetry analysis and calculation results for the Te moments induced in the magnon states. In the calculations, each magnon is characterized by its own electron band structure. We investigate the transformation of the electron structure in the transition of the material from the collinear ground state to noncollinear magnon states. We show the connection between the properties of magnon band structures and the chirality properties of magnons. In the investigation of the chirality splitting as well as in both the formulation and the application of our method, an important role play the aspects of generalized symmetry based on the application of the spin-space groups. The symmetry framework connects in one coherent picture different parts of the consideration: (i) the generalized translational symmetry of the magnons as a crucial condition for their efficient *ab initio* calculation, (ii) altermagnetic spin splitting of the electron states in the ground state, and (iii) chirality splitting and band structures of the magnon excitations.

DOI: [10.1103/PhysRevB.111.184436](https://doi.org/10.1103/PhysRevB.111.184436)

## I. INTRODUCTION

Magnons as low-energy excitations of the magnetic systems play a central role in the magnetic thermodynamics. The emerging field of magnonics enhanced further the importance of the magnons [1–4]. The first-principles study of the magnons is one of the prominent tasks of the theoretical approaches to magnetic systems based on the density functional theory (DFT).

In the adiabatic picture focusing on the dynamics of atomic magnetic moments, the magnons are presented by the configurations of the moments deviating from the magnetization axis [5–7]. The structure of a magnon is characterized by the wave vector and by the angles specifying the deviation of the atomic moments from the magnetization axis. For an elemental

ferromagnet (FM) with one magnetic atom per the crystallographic unit cell the structure of the magnons is uniquely determined by the wave vector [Fig. 1(a)]. The deviation angle  $\theta$  is the same for all atoms. Therefore in this case only the energies of the magnons need to be determined. In more complex systems such as antiferromagnets (AFM) [Figs. 1(b) and 1(c)], ferrimagnets, or ferromagnets with several inequivalent atoms in the crystallographic unit cell, different atomic moments deviate differently from the magnetization axis and the determination of the structure of the magnons is an important part of the magnon study.

There are different approaches to the DFT based calculation of magnons. One of the approaches is the calculation of the dynamic magnetic susceptibility in nonuniform transversal magnetic field [8–14]. A strong feature of this method is that it allows to investigate not only the structure and the energy of magnons but also their life time resulting from the interaction of magnons with single-electron Stoner

\*Contact author: lsandr3591@gmail.com

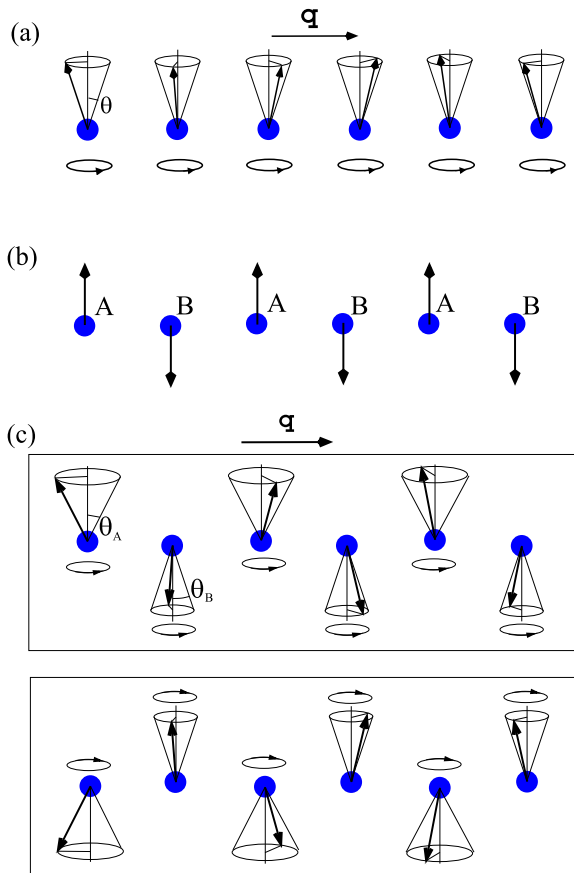


FIG. 1. (a) Schematic presentation of the spin waves in an elemental ferromagnet. (b) Schematic presentation of the ground state magnetic structure of a two sublattice AFM. Sublattices are marked by letters A and B. (c) Schematic presentation of the spin waves in a two sublattice AFM. Angles  $\theta_A$  and  $\theta_B$  give deviations of the atomic moments of the sublattices from the magnetization axis. (Top) Magnon of type A with  $\theta_A > \theta_B$ . (Bottom) Magnon of type B with  $\theta_B > \theta_A$ .

excitations. In the case of complex magnetic materials, the method is very demanding with respect to both computation techniques and computer resources. A widely used approach to the theoretical study of the adiabatic magnons is the mapping, as an intermediate step, of the electron system on the Heisenberg Hamiltonian of interacting atomic moments. Such a mapping is currently a standard procedure consisting in the DFT based evaluation of the Heisenberg exchange parameters (see, e.g., Refs. [15–22]). An efficient method of the mapping was suggested by Liechtenstein *et al.* [15] and is based on the evaluation of the variation of the band energy as the response to the infinitesimal deviation of the atomic moments from the magnetization axis. The possibility to replace the variation of the total energy by the variation of the band energy is based on so-called magnetic force theorem [15]. A recent review of the development and applications of the Liechtenstein *et al.* method is given in Ref. [23]. In this paper, we suggest a direct DFT-based method for the magnon calculation that does not include mapping of the electron system on the Heisenberg Hamiltonian. To our best knowledge, this is the first method allowing direct DFT calculations of adiabatic magnons in

complex collinear magnets. The method has important features not provided by the standard mapping approach. Among them are the following. First, the fully self-consistent calculation of the magnon structure and energy is performed in contrast to the mapping approach based on the evaluation of the band energy variation from non-self-consistent calculation. Second, in the magnon states of complex structures, the atoms that are equivalent in the ground state may become inequivalent. The suggested method takes this into account in a consequent self-consistent manner. Third, in the compounds, the contribution of the nominally nonmagnetic atoms to the magnon states is self-consistently taken into account. Forth, the method allows to estimate the dependence of the magnon energy on the number of magnons by varying the tilting angles of the atomic moments from the magnetization axis. The approach suggested by Liechtenstein *et al.* considers an infinitesimal deviation of the moments from the magnetization axis. Fifth, because of the exact treatment of the generalized periodicity of the helical magnetic structures with arbitrary wave vectors our method accounts for the exchange interactions between atoms at arbitrary large distances in contrast to the mapping calculations that often take into account only a few nearest neighbor interactions.

Since each magnon presents a different state of the system, the direct self-consistent calculation of a magnon state within the DFT framework must include constraints responsible for the convergence of the calculation to the desired magnetic state instead of the standard DFT convergence to the ground state (GS). Two different constraints are simultaneously used in the method. The first governs the change of the net magnetization. The method uses the formula

$$\omega = \frac{\Delta E}{\Delta m_z} \quad (1)$$

derived in Ref. [7] for the magnon energy in an arbitrary collinear magnet [24]. Here  $\Delta E$  is the increase of the energy of the magnon state with respect to the GS and  $\Delta m_z$  is the magnetization change with respect to the GS magnetization. Equation (1) correlates with the property that one magnon changes the magnetization of the system by  $1 \mu_B$ . The first constraint imposes the condition on the magnetization of the system by means of introduction of an effective magnetic field.

The second constraint specifies the value of the magnon wave vector. This is a symmetry type of constraint [25] where the invariance of the initial Hamiltonian with respect to the symmetry operation responsible for the desired property reproduces itself during iterations. The symmetry constraint does not need a constraining field. It is important to emphasize that to constrain the magnon wave vector the generalized translational periodicity described by the machinery of spin space groups (SSG) must be imposed. The combination of two different constraints is the characteristic feature of the method. In the paper, we formulate the method in the form valid for the study of the magnons in any collinear magnet without spin-orbit coupling (SOC). The performance of the method is demonstrated by the application to altermagnets focusing on MnTe as a representative of this class of materials. As the notion of an altermagnet is rather new it is worth to introduce it briefly. The ground state of a two sublattice AFM

is characterized by two mutually compensating ferromagnetic sublattices. In terms of the electron structure, the zero net magnetization of an AFM is the result of the mutual compensation of the spin-up and spin-down electron states which is the consequence of the symmetry properties of the material. Importantly, the realization of this spin compensation can be different for different AFM materials. It can take place either at each wave vector  $\mathbf{k}$  of the reciprocal space or, alternatively, between the electron states corresponding to different  $\mathbf{k}$  points. Šmejkal, Sinova, and Jungwirth [26,27] suggested the term *altermagnet* for the materials where the magnetic compensation takes place between different  $\mathbf{k}$  points. The absence of the spin degeneracy at the same  $\mathbf{k}$  point can be treated as the spin splitting of the electron states at this point. This property of altermagnets has important physical consequences attracting enormous research attention to this class of materials [27–33].

Among the special properties of altermagnets is the chirality splitting of the magnon states [22,29,34–36]. In Ref. [34], the presence of the magnon chirality splitting is connected with the properties of the Heisenberg exchange parameters. A general approach to the chirality splitting applicable in the DFT-based direct calculations has not yet been suggested. Also the discussion of the symmetry pattern of the magnon chirality splitting in the reciprocal wave-vector space and its relation to the symmetry pattern of the exchange splitting in the ground-state band structure is not available. To give the answers to these questions is one of the aims of this paper.

Each AFM magnon brings either positive or negative magnetization to the system. If in Fig. 1(c)  $\theta_A > \theta_B$  the magnon gives negative contribution to the magnetization whereas for a magnon with  $\theta_A < \theta_B$  the contribution to the magnetization is positive. These two types of magnons have opposite chiralities. The two types of magnons are obtained in both Heisenberg model (see, e.g., Ref. [37]) and first-principles calculation of the dynamical spin susceptibility (see, e.g., Ref. [10]). We will refer to these two types of magnons as magnons of type A and B according to the larger of two angles  $\theta_A$  and  $\theta_B$ . The net magnetization of an AFM at nonzero temperatures remains zero. This property is the consequence of the mutual compensation of the magnons of opposite chiralities which results from their symmetry-determined energy degeneracy. Again there are two possibilities. The chirality compensation can take place either at each magnon wave vector  $\mathbf{q}$  or only between magnons with different wave vectors. The latter situation takes place in altermagnets and may be referred to as chirality splitting of magnons with a given wave vector  $\mathbf{q}$ . The nature of the chirality degeneracy of the magnons is very different compared to the spin degeneracy of the electron states discussed above. However, in both cases, the two symmetry questions to address are similar. First, which symmetry operations are responsible for the degeneracy of the magnons with opposite chiralities, and, second, does the degeneracy take place between the magnons with the same wave vector or with different wave vectors? As will be demonstrated, the answers to these questions for magnons are closely related to those for the electron states.

Our choice of altermagnet MnTe as the object of the application of the method has following reasons. First, as a particular case of a two-sublattice AFM containing

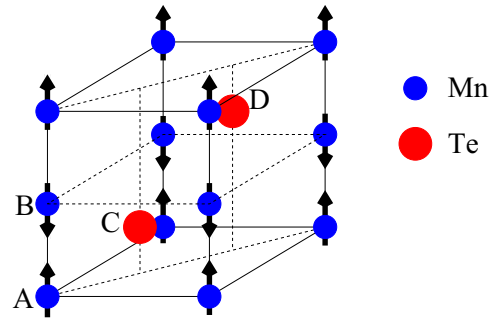


FIG. 2. Unit cell of AFM MnTe. Labeling A–D of the sublattices is used throughout the paper.

nonmagnetic atoms (Fig. 2), it is complex enough to demonstrate important features of the method. In the case of MnTe, the altermagnetic properties are the consequences of the presence of the Te atoms. Indeed, in an assumed material with removed Te atoms the altermagnetic spin and chirality splittings are absent. Due to the crucial role of Te atoms in altermagnetism, accounting for their self-consistent response to changes in the Mn subsystem is a key aspect. In this context, key questions to address include the questions of whether the Te atoms remain equivalent in the magnon states and of what symmetry arguments can reveal about the induced Te moments. The magnon-specific symmetry information about nonmagnetic atoms, besides its general physical importance, helps to control and accelerate the convergence of the magnon calculation. These “technical” advantages from the symmetry analysis are discussed in Sec. IV D.

Next question addressed in the paper is how the chirality properties of the magnon states of the system are related to the properties of the electron band structures of the magnon states. To our best knowledge, this is the first study of this type. It is based on the possibility to calculate the band structure of the magnon states opened by our method. The deep connection between two different energy characteristics of altermagnets, magnon energies and magnon electron band structures, is exposed.

As seen from the above, the symmetry aspects play in the paper an important role. There are three different parts of the work where the symmetry arguments are essential: (i) the formulation of the method of the direct magnon calculation, (ii) the study of the spin splitting of the electron states in the GS of an altermagnet, and (iii) the study of the chirality splitting of the spin waves in an altermagnet. The employment of the SSG allows both solving these tasks and the integration of different parts of the study in one coherent physical picture. We consider this coherent picture uniting very different sides of the consideration as one of important results of the paper. As discussed below, in part (ii), the employment of usual space groups can be technically sufficient. In other parts and in the formation of a general picture, the use of the generalized spin-space groups is essential.

The paper is structured as follows. In Sec. II, the method of direct DFT based calculation of magnon states is presented. Section III gives the details of the calculations. In Sec. IV, the symmetry aspects and the results of the calculations are discussed. This section includes a brief introduction of the SSGs

(Sec. IV A), discussion of the spin degeneracy and altermagnetic spin splitting of the electron states in AFM (Sec. IV B), application to the electron states of MnTe (Sec. IV C), discussion of the symmetry governed properties of the magnetic sublattices in the magnon states (Sec. IV D), and of the chirality splitting of magnons in altermagnets (Sec. IV E), results of the calculation of magnon dispersion (Sec. IV F), brief discussion of the noticed instability cases of magnon state energy with respect to the number of magnons (Sec. IV G), and the study of the relation between electronic band structures of the magnon states and chirality properties of these states (Sec. IV H). Section V is devoted to the conclusions.

## II. THE METHOD OF DIRECT DFT-BASED MAGNON CALCULATION

As mentioned in the introduction, in Ref. [7], it was shown that for any collinear magnet the magnon energy can be presented within the framework of the DFT theory in the form given by Eq. (1) (see also Ref. [24]). The value of  $\Delta m_z$  corresponds to the number of magnons with given wave vector and  $\Delta E$  is their energy. It is expected that there is an interval of  $\Delta m_z$  where  $\Delta E$  is proportional to  $\Delta m_z$  and the calculation for any  $\Delta m_z$  from this interval gives the value of the spin wave energy. The both quantities can be considered per unit cell. To obtain the self-consistent magnon state with a given magnetization  $m_0 - \Delta m_z$ , the minimization of the density functional must be performed under the constraining condition

$$\int d\mathbf{r} m_z(\mathbf{r}) = m_0 - \Delta m_z. \quad (2)$$

Here  $m_0$  is the ground state magnetization that is zero in the case of an AFM.

The constrained energy functional takes the form

$$E_{\text{const}}[n, \mathbf{m}] = E[n, \mathbf{m}] + h \left[ \int d\mathbf{r} m_z(\mathbf{r}) - m_0 + \Delta m_z \right], \quad (3)$$

where  $E[n, \mathbf{m}]$  is unconstrained functional, Lagrange parameter  $h$  plays the role of the  $z$  component of an effective magnetic field  $\mathbf{h} = (0, 0, h)$ . The condition on the magnetization [Eq. (2)] is the same for all magnons independent of their wave vectors whereas the value of field  $h$  corresponding to a given  $\Delta m_z$  is  $\mathbf{q}$  dependent. In systems with well defined atomic moments considered in the paper, field  $\mathbf{h}$  governs the values of the deviations of the moments from the  $z$  axis. For each magnetic atom, the vector of the constraining field  $\mathbf{h}$  can be decomposed into two components: one collinear to the moment and the other orthogonal to it (Fig. 3). The component collinear to the moment influences the value of the moment. This influence is weak for well defined atomic moments since the variation of the value of the moments is energetically costly. In this case, the orthogonal component plays the main role governing the deviation of the moments from the magnetization axis and leading to the desired magnetization change  $\Delta m_z$ . The orthogonal components form nonuniform magnetic field with wavelength identical to the wavelength of the magnon. The second constraint specifying the wave vector  $\mathbf{q}$  of the magnon reflects the generalized periodicity

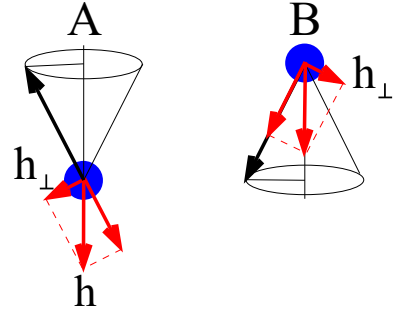


FIG. 3. Schematic picture of the decomposition of the constraining field  $\mathbf{h}$  into two components: one collinear to the moment and the other,  $\mathbf{h}_\perp$ , orthogonal to it. The left (right) part of the figure shows the decomposition for atoms of sublattice A (B). The field is antiparallel to the  $z$  axis and leads to the magnon state assigned to sublattice A. For magnons of type B, the direction of field  $\mathbf{h}$  is opposite.

[38] of the helix with given  $\mathbf{q}$

$$\{\alpha_{\mathbf{qn}}|E|\mathbf{R}_n\}\mathbf{m}(\mathbf{r}) \equiv \alpha_{\mathbf{qn}}\mathbf{m}(\mathbf{r} - \mathbf{R}_n) = \mathbf{m}(\mathbf{r}). \quad (4)$$

Here  $\{\alpha_{\mathbf{qn}}|E|\mathbf{R}_n\}$  are the operators of generalized translations consisting from the lattice translation  $\mathbf{R}_n$  accompanied by the rotation of magnetization by angle  $\mathbf{q}\mathbf{R}_n$  about the  $z$  axis.  $E$  in the second position in the symmetry operator means that the operator does not perform any point transformation besides the magnetization rotation. The Kohn-Sham equation of a helical structure in external field  $\mathbf{h}$  takes the form

$$\hat{\mathbf{H}} \begin{pmatrix} \psi_+ \\ \psi_- \end{pmatrix} = E \begin{pmatrix} \psi_+ \\ \psi_- \end{pmatrix} \quad (5)$$

with Hamiltonian

$$\hat{\mathbf{H}} = \hat{\mathbf{T}} \begin{pmatrix} 1 & 0 \\ 0 & 1 \end{pmatrix} + \sum_{nv} \mathbf{U}^+(\theta_v, \phi_{nv}) \mathbf{V}_v(\mathbf{r}_{nv}) \mathbf{U}(\theta_{nv}, \phi_{nv}) + h\sigma_z, \quad (6)$$

where  $\hat{\mathbf{T}}$  is the operator of kinetic energy,  $n$  numbers unit cells,  $v$  numbers atomic sublattices,  $\mathbf{V}_v$  is two by two potential of the  $v$ th atom in the local atomic spin coordinate system,  $\mathbf{r}_{nv} = \mathbf{r} - \mathbf{a}_v - \mathbf{R}_n$ ,  $\mathbf{a}_v$  gives the position of the  $v$ th atom in the unit cell, angles  $\theta_v$  and  $\phi_{nv}$  specify the direction of the moment of the  $nv$ th atom,  $\phi_{nv} = \phi_v + \mathbf{q}\mathbf{R}_n$ ,  $\mathbf{U}(\theta_{nv}, \phi_{nv})$  is the standard spin- $\frac{1}{2}$ -rotation matrix, and  $\sigma_z$  is the Pauli matrix. The action of the generalized translation on the spinor wave function  $\Psi(\mathbf{r}) = \begin{pmatrix} \psi_+(\mathbf{r}) \\ \psi_-(\mathbf{r}) \end{pmatrix}$  has the form

$$\{\alpha_{\mathbf{qn}}|E|\mathbf{R}_n\}\Psi(\mathbf{r}) = \mathbf{U}(\alpha_{\mathbf{qn}})\Psi(\mathbf{r} - \mathbf{R}_n). \quad (7)$$

The Hamiltonian of a  $\mathbf{q}$ -magnon [Eq. (6)] commutes with generalized translations corresponding to given  $\mathbf{q}$  [39,40]. The symmetry properties of the Hamiltonian govern the symmetry properties of the calculated electron states that leads to the reproduction of the generalized translational symmetry of the Kohn-Sham Hamiltonian during iterations. Because of this, the fulfillment of the symmetry constraint [Eq. (4)] does not require application of a constraining field.

The symmetry with respect to the generalized translations fulfills the conditions of the generalized Bloch theorem and



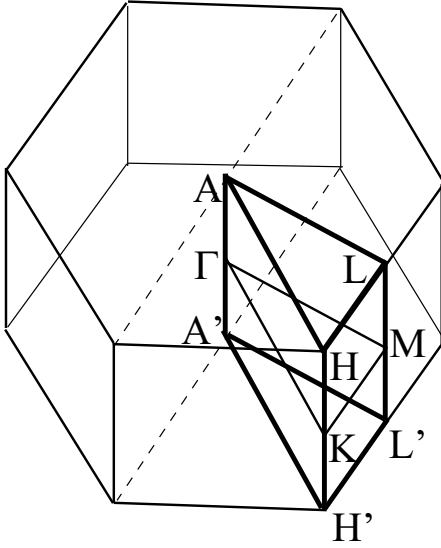


FIG. 4. Brillouin zone and irreducible domain for calculation of both electronic band structure of the AFM GS in the  $\mathbf{k}$  space and spin waves in the  $\mathbf{q}$  space.

allows an exact reduction of the calculation for the spiral structure with arbitrary wave vector to the consideration of the small crystallographic unit cell of the crystal [39].

### III. CALCULATION DETAILS

The calculations were performed with the augmented spherical waves (ASW) method [41,42]. The local density approximation (LDA) to the exchange-correlation functional is used [43]. The account for generalized translation symmetry and external magnetic field have been implemented earlier [44,45]. Therefore only limited adaptation of the code were needed. The calculations were performed with three different  $\mathbf{k}$  meshes in the Brillouin zone (BZ) of the material (Fig. 4):  $n \times n \times n$ ,  $n = 10, 20$ , and  $30$ . Here  $n$  is the number of the intervals in which the primitive vectors of the reciprocal lattice were divided. The results of the calculations have shown that the difference between spin wave energies obtained with  $n = 20$  and  $30$  is usually small and most of the calculations reported in the paper were performed with  $n = 20$ . In the calculations, we used experimental lattice parameters [56]  $a = 4.15 \text{ \AA}$  and  $c = 6.71 \text{ \AA}$ . As mentioned above, a straightforward application of Eq. (1) assumes the existence of an interval of  $\Delta m_z$  where energy increase  $\Delta E$  is proportional to magnetization change  $\Delta m_z$ . Our calculations confirmed that usually such a linear dependence exists up to rather large deviation angles of the Mn atomic moments from the magnetization axis. Figure 5 shows typical characters of the dependences between calculated quantities and demonstrates high stability of the calculated magnon energy with respect to the value of the deviation of the Mn moments from the magnetization axis. The results of the calculations presented in the figure were obtained for wave vector  $\mathbf{q} = (0,0,0.3)$ . Here and in the rest of the paper we give the  $x$  and  $y$  components of the reciprocal space vectors in units of  $\frac{2\pi}{a}$  and the  $z$  components in units of  $\frac{2\pi}{c}$ . We calculated constraining

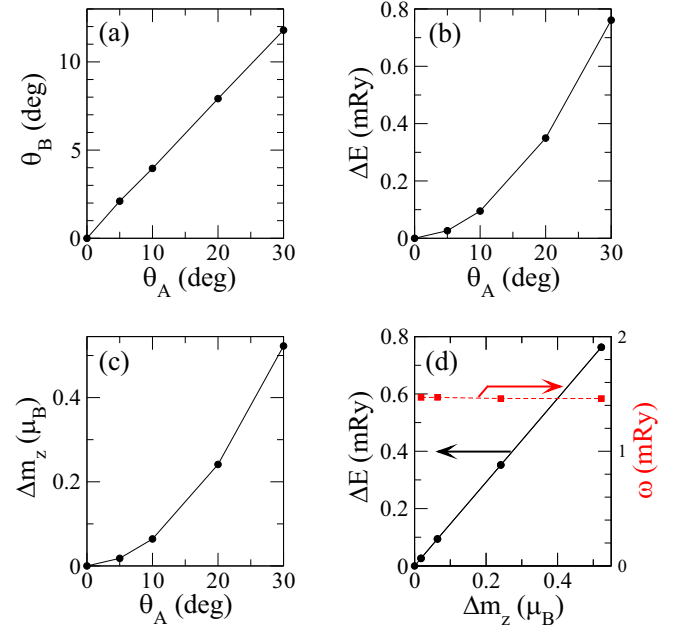


FIG. 5. The dependence of  $\Delta E$  on  $\Delta m_z$ . Figure shows calculations performed for magnon with wave vector  $\mathbf{q} = (0,0,0.3)$ . [(a)–(c)] The dependencies of, respectively,  $\theta_B$ ,  $\Delta E$ , and  $\Delta m_z$  on  $\theta_A$ . (d) The dependence of energy increase  $\Delta E$  (black circles, left energy scale) and magnon energy  $\omega$  (red squares, right energy scale) on  $\Delta m_z$ .

field  $h$  stabilizing the deviations of the Mn moments of sublattice A at following values:  $\theta_A = 5^\circ, 10^\circ, 20^\circ, 30^\circ$ . Figure 5(a) gives calculated deviations of the moments of sublattice B,  $\theta_B$ . Figure 5(b) shows corresponding increase in energy  $\Delta E$ . The difference between  $\theta_A$  and  $\theta_B$  is the source of the magnetization change  $\Delta m_z$  shown in Fig. 5(c). In Fig. 5(d), we present the dependence of  $\Delta E$  on  $\Delta m_z$  which is very close to a linear one. The ratio of these quantities giving the magnon energy is with a good accuracy independent of  $\Delta m_z$ . In most of the calculations presented in the paper, we used  $\theta_A = 20^\circ$ . On the other hand, performing model calculations aimed at testing our method we obtained also the cases where strong deviation from the simple dependence of  $\Delta E$  on the deviation angle of the Mn atomic moments was registered showing the capacity of the method to reveal an instability connected with the deviation of the atomic moments from the magnetization axis. These results are briefly presented in Sec. IV G. In these calculations we used the LDA +  $U$  approach in the flavor of Dudarev *et al.* [46].

### IV. SYMMETRY ASPECTS AND RESULTS OF CALCULATIONS

#### A. SSG groups

The standard tool for the analysis of the symmetry properties of the crystalline materials is the apparatus of space groups. For magnetic systems an antisymmetry operation is included into consideration making extension from space groups to magnetic space groups [47,48]. The antisymmetry operation that in an abstract treatment can be considered as changing the color between black and white in the magnetic

case is responsible for the reversal of the magnetization direction by means of time reversal. However, in the problems where the influence of the SOC can be neglected, this tool is not sufficient for the description of the properties of magnetic systems. In particular, these limitations have been revealed for both electron band structure calculations and the studies based on the Heisenberg Hamiltonian of interacting atomic moments.

The solution of the problem has been found in the concept of SSG whose elements allow different transformation of the spin and space variables (see, e.g., Refs. [49–51]). In recent years the interest to SSG has been revived. Reference [52] reports a detailed analysis of the magnon band topology within the framework of the Heisenberg and Heisenberg-Kitaev models of interacting atomic moments. Very recently several systematic works [53–55] were published devoted to the classification, properties, and applications of the SSGs.

The action of the SSG operator  $\{\alpha_S|\alpha_R|\boldsymbol{\tau}\}$  on the magnetization  $\mathbf{m}(\mathbf{r})$  is defined as

$$\{\alpha_S|\alpha_R|\boldsymbol{\tau}\}\mathbf{m}(\mathbf{r}) = \alpha_S\mathbf{m}([\alpha_R|\boldsymbol{\tau}]^{-1}\mathbf{r}), \quad (8)$$

where  $\alpha_S$  and  $\alpha_R$  are spin and space rotations respectively,  $\boldsymbol{\tau}$  is space translation, and we introduced notation  $[\alpha_R|\boldsymbol{\tau}] \equiv \{E|\alpha_R|\boldsymbol{\tau}\}$ . The action of the SSG operator on the two-component spinor has the form

$$\{\alpha_S|\alpha_R|\boldsymbol{\tau}\}\Psi(\mathbf{r}) = \mathbf{U}(\alpha_S)\Psi([\alpha_R|\boldsymbol{\tau}]^{-1}\mathbf{r}). \quad (9)$$

The generalized translations [Eq. (7)], crucial for the study of spiral magnetic configurations, are the operations of the SSG. The operation of time reversal acting on two-component spinor takes the form

$$\Theta = -i\sigma_y K = \begin{pmatrix} 0 & -1 \\ 1 & 0 \end{pmatrix} K, \quad (10)$$

where  $K$  is the operator of complex conjugation. Since  $\begin{pmatrix} 0 & -1 \\ 1 & 0 \end{pmatrix}$  belongs to the set of unitary matrices  $\mathbf{U}$  entering Eq. (9), it already belongs to the SSG as an operation providing a spin rotation. Therefore the complex conjugation  $K$  is also an allowed SSG operation. This means that the real form of the Kohn-Sham equations of collinear magnets [Eq. (6)] and its consequences become within SSGs a part of a straightforward symmetry treatment.

The effectiveness of applying SSG, compared to space groups, can be characterized as follows. The neglect of the SOC leads effectively to the replacement of the actual physical 3D space by the 6D space where spin and orbital variables are independent and can be transformed separately. The account for this freedom gives important new information about the properties of the system. In addition, the SSGs allow a straightforward establishment of continuity relations between theoretical results obtained within different approximations, such as with and without SOC, or between the results obtained for collinear and helical magnetic configurations. The reason for this is the property that the SSG of the less symmetric case is the subgroup of the SSG of the more symmetric case. The latter feature plays important role in Sec. IV H where we discuss the transformation path of the electron band structure of a collinear magnet to the electron band structure of a magnon with a given wave vector  $\mathbf{q}$ .

Summarizing the applications in the paper of the symmetry concepts, we distinguish three different problems. The first was considered in Sec. II and uses the generalized translations as a symmetry constraint in the calculation of the magnon states. The second and third are, respectively, the alternmagnetic spin-splitting of the electron states and chirality splitting of the magnon states.

## B. Degeneracy of the electron states in collinear magnets

The material of this section contributes to making the paper reasonably self-contained and provides the basis for the comparison with the results on the magnon chirality splitting discussed in Sec. IV E.

The electronic band structure of collinear magnets has been calculated already for distinctly more than 50 years (see, e.g., Refs. [57,58]). The electron wave functions were treated as scalar functions labeled with an index specifying the sign of the spin projection on the selected quantization axis. Respectively, two scalar Schrödinger equations were considered, one for each spin projection. The symmetry-caused degeneracy of the electron states arises in the following way. If  $g = [\alpha_R|\boldsymbol{\tau}]$  is a symmetry operation commuting with a scalar Schrödinger equation, the action of this operation on an eigenstate  $\psi_{\mathbf{k}\sigma}$  gives the eigenstate with the same energy, the same spin projection  $\sigma$ , and wave vector  $\alpha_R\mathbf{k}$ . The real form of the equation additionally gives the degeneracy of the electron states at points  $\mathbf{k}$  and  $-\mathbf{k}$ . The different vectors from the list of all  $\alpha_R\mathbf{k}$  and  $-\alpha_R\mathbf{k}$  vectors form the star  $\{\mathbf{k}\}$  of vector  $\mathbf{k}$  [59].

In a FM, the Schrödinger equations for opposite spin projections are essentially different and, therefore, there is no symmetry-caused degeneracy of the spin-up and spin-down states. The spin splitting is the term characterizing this property of the electron structure which is valid for each point of the  $\mathbf{k}$  space.

On the other hand, in an AFM, there must be degeneracy between the states with opposite spin projections. This degeneracy is the reason for the zero net magnetization of the AFM. To expose the origin of the spin degeneracy we first notice that in the Schrödinger equation for electrons with a given spin projection  $\sigma$  the electrons see different potentials at the atoms of different magnetic sublattices. Therefore, at the first step, only the operations leaving the sublattices invariant are considered. For each vector  $\mathbf{k}$  they give star  $\{\mathbf{k}\}_{\text{subl}}$  corresponding to the symmetry group of the sublattices. Next it is necessary to specify the symmetry operation that transforms the equations corresponding to different spin projections into each other. The real-space part of this operation  $[\alpha_R^{tr}|\boldsymbol{\tau}]$  must transform the sublattices into each other and be accompanied by an “antisymmetry” operation  $E'$  reversing the signs of the spin indices. The physical nature of this antisymmetry operation is time reversal. As a consequence of such symmetry operation any spin-up state at point  $\mathbf{k}$  is degenerate with a spin-down state at  $\alpha_R^{tr}\mathbf{k}$ . This makes the system as a whole spin-compensated. The answer to the question whether the spin compensation takes place at each  $\mathbf{k}$  point of the BZ or only between different  $\mathbf{k}$  points depends on the properties of operation  $[\alpha_R^{tr}|\boldsymbol{\tau}]$  transforming the sublattices into each other. If vector  $\alpha_R^{tr}\mathbf{k}$  belongs to star  $\{\mathbf{k}\}_{\text{subl}}$  the degeneracy takes place at each  $\mathbf{k} \in \{\mathbf{k}\}_{\text{subl}}$ . In the opposite case, we deal with an alternmagnet with spin splitting at all points of the star  $\{\mathbf{k}\}_{\text{subl}}$ .

TABLE I. Point symmetry elements. The following notations are used:  $E$  is the unity transformation,  $I$  is the space inversion,  $C_n^m$  is the rotation by angle  $2\pi \frac{m}{n}$ . In the column “axis,” the unit vectors parallel to the rotation axes are given. The two operations presented in each row have the same rotation axes. Columns headed  $\alpha_R \mathbf{r}$  and  $I\alpha_R \mathbf{r}$  give the coordinates of the vectors obtained after rotation of vector  $\mathbf{r} = (x, y, z)$ . In columns headed  $\tau$ , symbol marks the symmetry operations containing nonprimitive translation  $\tau = (0, 0, 0.5)$ . In the columns headed “subl,” the operations transforming the Mn sublattices into themselves are marked with  $\cdot$ . For all direct-space vectors, the  $x$  and  $y$  coordinates are given in units of lattice parameter  $a$  and the  $z$  coordinate in units of lattice parameter  $c$ .

$N$	$\alpha_R$	axis	$\alpha_R \mathbf{r}$			$\tau$	subl	$N$	$I\alpha_R$	$I\alpha_R \mathbf{r}$			$\tau$	subl
1	$E$		$x$	$y$	$z$	—	✓	13	$I$	$-x$	$-y$	$-z$	—	✓
2	$C_6^1$	(0,0,1)	$\frac{1}{2}x - \frac{\sqrt{3}}{2}y$	$\frac{\sqrt{3}}{2}x + \frac{1}{2}y$	$z$	✓	—	14	$IC_6^1$	$-\frac{1}{2}x + \frac{\sqrt{3}}{2}y$	$-\frac{\sqrt{3}}{2}x - \frac{1}{2}y$	$-z$	✓	—
3	$C_6^5$	(0,0,1)	$\frac{1}{2}x + \frac{\sqrt{3}}{2}y$	$-\frac{\sqrt{3}}{2}x + \frac{1}{2}y$	$z$	✓	—	15	$IC_6^5$	$-\frac{1}{2}x - \frac{\sqrt{3}}{2}y$	$\frac{\sqrt{3}}{2}x - \frac{1}{2}y$	$-z$	✓	—
4	$C_6^2$	(0,0,1)	$-\frac{1}{2}x - \frac{\sqrt{3}}{2}y$	$\frac{\sqrt{3}}{2}x - \frac{1}{2}y$	$z$	—	✓	16	$IC_6^2$	$\frac{1}{2}x + \frac{\sqrt{3}}{2}y$	$-\frac{\sqrt{3}}{2}x + \frac{1}{2}y$	$-z$	—	✓
5	$C_6^4$	(0,0,1)	$-\frac{1}{2}x + \frac{\sqrt{3}}{2}y$	$-\frac{\sqrt{3}}{2}x - \frac{1}{2}y$	$z$	—	✓	17	$IC_6^4$	$\frac{1}{2}x - \frac{\sqrt{3}}{2}y$	$\frac{\sqrt{3}}{2}x + \frac{1}{2}y$	$z$	—	✓
6	$C_6^3$	(0,0,1)	$-x$	$-y$	$z$	✓	—	18	$IC_6^3$	$x$	$y$	$-z$	✓	—
7	$C_2$	(1,0,0)	$x$	$-y$	$-z$	—	✓	19	$IC_2$	$-x$	$y$	$z$	—	✓
8	$C_2$	( $\frac{1}{2}, \frac{\sqrt{3}}{2}, 0$ )	$-\frac{1}{2}x + \frac{\sqrt{3}}{2}y$	$\frac{\sqrt{3}}{2}x + \frac{1}{2}y$	$-z$	—	✓	20	$IC_2$	$\frac{1}{2}x - \frac{\sqrt{3}}{2}y$	$-\frac{\sqrt{3}}{2}x - \frac{1}{2}y$	$z$	—	✓
9	$C_2$	( $-\frac{1}{2}, \frac{\sqrt{3}}{2}, 0$ )	$-\frac{1}{2}x - \frac{\sqrt{3}}{2}y$	$-\frac{\sqrt{3}}{2}x + \frac{1}{2}y$	$-z$	—	✓	21	$IC_2$	$\frac{1}{2}x + \frac{\sqrt{3}}{2}y$	$\frac{\sqrt{3}}{2}x - \frac{1}{2}y$	$z$	—	✓
10	$C_2$	( $\frac{\sqrt{3}}{2}, \frac{1}{2}, 0$ )	$\frac{1}{2}x + \frac{\sqrt{3}}{2}y$	$\frac{\sqrt{3}}{2}x - \frac{1}{2}y$	$-z$	✓	—	22	$IC_2$	$-\frac{1}{2}x - \frac{\sqrt{3}}{2}y$	$-\frac{\sqrt{3}}{2}x + \frac{1}{2}y$	$z$	✓	—
11	$C_2$	(0,1,0)	$-x$	$y$	$-z$	✓	—	23	$IC_2$	$x$	$-y$	$z$	✓	—
12	$C_2$	( $-\frac{\sqrt{3}}{2}, \frac{1}{2}, 0$ )	$\frac{1}{2}x - \frac{\sqrt{3}}{2}y$	$-\frac{\sqrt{3}}{2}x - \frac{1}{2}y$	$-z$	✓	—	24	$IC_2$	$-\frac{1}{2}x + \frac{\sqrt{3}}{2}y$	$\frac{\sqrt{3}}{2}x + \frac{1}{2}y$	$z$	✓	—

This approach to the symmetry properties of AFMs allows to reach the description of the electron structure without reference to the SSG. Its application to MnTe was reported in old publication Ref. [60]. A very detailed and complete discussion of the application of this type of approach to the altermagnets was recently published by Turek [61]. This approach has shortcomings: Instead of treating the electron wave functions as spinors it considers them as scalars labeled with a spin index. This complicates the consideration of the influence on the electron band structure of the SOC or of the noncollinearity of the magnetic configuration where the account for spinor form of the electron wave functions is essential. Therefore this approach is not sufficient for the purposes of this paper where noncollinear incommensurate spiral structures are in the focus of the consideration.

The application of the SSG to the symmetry analysis of the collinear magnetic structures gives additional useful features. First, any spin rotation  $\{C_{z\phi}|E|0\}$  about the  $z$  axis is a symmetry operation of the spinor Kohn-Sham equation [Eqs. (5) and (6)]. As the consequence of this symmetry the electron eigenfunctions assume one of the two spinor forms  $\psi(\mathbf{r})_{(0)}^{(1)}$  or  $\psi(\mathbf{r})_{(1)}^{(0)}$  corresponding to different irreducible representations (IR) of the SSG group [62]. Therefore the spin-indexing of the electron functions is now a straightforward consequence of the symmetry of the problem and not the property imposed on the basis of additional arguments. Another consequence of the description of the collinear magnetic states in terms of SSG is that these states can be treated as spiral structures with arbitrary wave vectors  $\mathbf{q}$  and deviation angles  $\theta = 0$ . Indeed, the group of generalized translations  $\mathbf{T}_{\mathbf{q}}$  with any  $\mathbf{q}$  is a subgroup of the group  $\mathbf{C}_z \times \mathbf{T}$  where  $\mathbf{T}$  is the group of space translations  $[E|\mathbf{R}_n]$  and  $\mathbf{C}_z$  is the group of all spin rotations  $C_{z\phi}$  about the  $z$  axis. This property will be used in Sec. IV H to study the transformation path of the electron

structure of the collinear ground state into the electron structure of the magnon state with a given wave vector.

### C. Collinear AFM ground state of MnTe

In MnTe, the space group of the atomic lattice contains 24 point operations listed in Table I: 12 operations of type I transform the Mn sublattices into themselves whereas other 12 operations of type II transform them into each other. In the AFM state, the point operations of type II remain the part of the symmetry operations in combination with spin-index reversal operation (time reversal operation).

The application of the 12 operations of type I to a reciprocal-space vector  $\mathbf{k} = (k_x, k_y, k_z)$  gives the set of 12 vectors with coordinates transformed according to the three columns of Table I with common heading  $\alpha_R \mathbf{r}$  or  $I\alpha_R \mathbf{r}$ . For instance, for the operation number 4, the transformed vector is  $(-\frac{1}{2}k_x - \frac{\sqrt{3}}{2}k_y, \frac{\sqrt{3}}{2}k_x - \frac{1}{2}k_y, k_z)$ . These 12 vectors are not necessarily different. For the most symmetric  $\Gamma$  point  $\mathbf{k} = (0, 0, 0)$  all vectors are equal and the corresponding star  $\{\mathbf{k}\}_{\text{subl}}$  consists of one vector. On the other hand, for a general point  $\mathbf{k}$  all 12 vectors are different. In Fig. 6, the points of the star  $\{\mathbf{k}\}_{\text{subl}}$  are shown for a general vector  $\mathbf{k}_0 = (k_{0x}, k_{0y}, k_{0z})$  and marked as black circles: 6 points lie in the  $k_z = k_{0z}$  plane and other 6 points in the  $k_z = -k_{0z}$  plane. At 12 points of the star  $\{\mathbf{k}_0\}_{\text{subl}}$  thus obtained, for each electron state at point  $\mathbf{k}_0$  there are equivalent states with the same energy and the same spin projection.

As a representative of the operations of type II we will use the reflection in the  $xy$  plane (operation number 18 in Table I). Action with this operation on the vectors of the star  $\{\mathbf{k}_0\}_{\text{subl}}$  gives another 12 vectors shown in Fig. 6 as red squares. They differ from the vectors of the star  $\{\mathbf{k}_0\}_{\text{subl}}$  by the sign of the  $z$  component. The states at these 12 vectors are degenerate

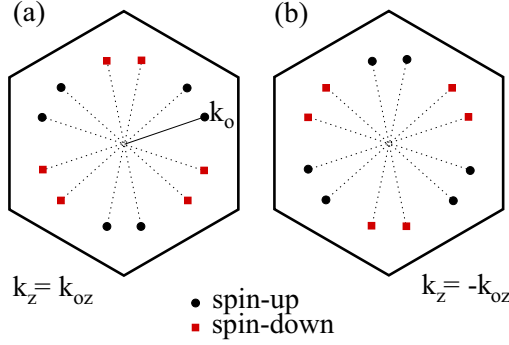


FIG. 6. Star  $\{\mathbf{k}_o\}$  of a general wave vector  $\mathbf{k}_o$ . The star contains 24 points lying in two planes  $k_z = k_{oz}$  [panel (a)] and  $k_z = -k_{oz}$  [panel (b)]. For any electron state at  $\mathbf{k}_o$ , the points shown by black circles contain equivalent states with the same spin projection. These 12 points form the star  $\{\mathbf{k}_o\}_{\text{subl}}$  corresponding to the symmetry group of the Mn sublattices. The points shown by red squares contain equivalent electron states with opposite spin projection. At all 24 points there is the altermagnetic spin splitting of the electron states. As discussed in Sec. IV E, the same figures reflect the properties of the chirality splitting of the magnons. In this case, the wave vectors  $\mathbf{k}$  of the electron states must be replaced by corresponding magnon wave vectors  $\mathbf{q}$  and references to spin projections by references to chiralities.

with the states at  $\mathbf{k}_o$  but have opposite spin projection. All 24 vectors are different and form full star  $\{\mathbf{k}_o\}$  of vector  $\mathbf{k}_o$ .

In general, for any  $\mathbf{k}$ , we have the star  $\{\mathbf{k}\}_{\text{subl}}$  obtained with operation leaving magnetic sublattices invariant and the full star  $\{\mathbf{k}\}$  obtained with account for all symmetry operations. These two sets of vectors are either identical or the number of vectors in  $\{\mathbf{k}\}$  is double. In the former case, the change of the sign of the  $z$  component of the vectors from  $\{\mathbf{k}\}_{\text{subl}}$  does not change the set of vectors and at all points of the set there is spin degeneracy of the electron states whereas in the latter case at all points in  $\{\mathbf{k}\}$  there is the altermagnetic spin splitting.

The irreducible domain of the AFM MnTe is the triangular prism  $\Gamma\text{MKALH}$  that is  $\frac{1}{24}$ th of the BZ (Fig. 4). The analysis of all points of the irreducible domain shows that the altermagnetic spin splitting takes place at all inner points of the prism and, additionally, at inner points of the face  $\Gamma\text{MLA}$ . At these points the calculations should be performed separately for the spin-up and spin-down states. Alternatively, the calculations can be performed in the  $\frac{1}{12}$ th of the BZ, prism  $\text{ALHA}'\text{L}'\text{H}'$  (Fig. 4), but for one spin projection only.

In Fig. 7, we show one fragment of the calculated band structure with spin-degenerate bands and one fragment with altermagnetic spin-splitting.

#### D. Magnetic structure of sublattices in magnon states

Let us discuss the properties of the structure of the AFM magnons that follow from the symmetry arguments. These results provide important general knowledge about properties of magnons. Simultaneously, they can be used in setting up and control of the DFT-based calculations. For example, the correlation in the directions of the atomic moments of different atoms predicted by symmetry must be present in the self-consistent solution for the magnon state that provides a

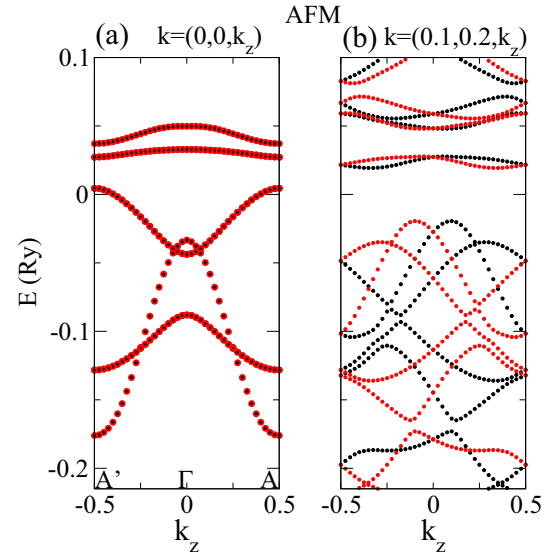


FIG. 7. Two fragments of the band structure of AFM MnTe. (a) High-symmetry line  $(0,0,k_z)$  in the reciprocal space. (b) Low-symmetry line  $(0.1,0.2,k_z)$  in the reciprocal space. Black (red) circles present spin-up (spin-down) states. At the points of the high-symmetry line all states are spin degenerate. In the case of the low-symmetry line, there is altermagnetic spin splitting at all points with exception of the center and end points of the interval.

tool for controlling the calculations. On the other hand, such a correlation can be used from the beginning of calculations to decrease the number of degrees of freedom and simplify the process of convergence. In addition, the symmetry-based knowledge that the magnetic atoms become inequivalent in the magnon excitations helps to avoid an unphysical assumption of the preserved equivalence of atoms and an erroneous constraint of the equivalence of magnetic atoms in the calculations.

We consider the magnon with an arbitrary wave vector  $\mathbf{q}$ . The magnetic structure of the magnon is invariant with respect to the generalized translations corresponding to given  $\mathbf{q}$ . As stated above, the direct magnon calculation includes an effective magnetic field acting on both magnetic sublattices. This field is collinear to the  $z$  axis and therefore parallel to the magnetization of one sublattice and antiparallel to the magnetization of the other sublattice [63]. Hence the atoms of the two sublattices in the magnon state become inequivalent. On the basis of these conclusions, the magnetic configurations of the two sublattices in a magnon state can be written in the following form

$$\mathbf{m}_{nA} = m_A \{ \sin(\theta_A) \cos[\mathbf{q}(\mathbf{a}_A + \mathbf{R}_n)], \sin(\theta_A) \times \sin[\mathbf{q}(\mathbf{a}_A + \mathbf{R}_n)], \cos(\theta_A) \}, \quad (11)$$

$$\mathbf{m}_{nB} = m_B \{ \sin(\pi - \theta_B) \cos[\mathbf{q}(\mathbf{a}_B + \mathbf{R}_n) + \pi + \phi], \sin(\pi - \theta_B) \sin[\mathbf{q}(\mathbf{a}_B + \mathbf{R}_n) + \pi + \phi], -\cos(\theta_B) \}. \quad (12)$$

Because of the inequivalence of the sublattices it is expected that  $m_A \neq m_B$ ,  $\theta_A \neq \theta_B$ , and there is an unknown not symmetry-governed angle  $\phi$  specifying the phase shift between  $xy$ -projections of the moments of the two sublattices.



The calculations with the suggested method confirmed that  $m_A \neq m_B$  and  $\theta_A \neq \theta_B$ . More details on these quantities will be given below.

However, concerning angle  $\phi$  the results of the calculations were unexpected: iterations started with an arbitrary selected  $\phi \neq 0$  resulted in the self-consistent magnetic configurations with  $\phi = 0$ . The question arises why the orientations of the moments of two inequivalent sublattices not connected by any symmetry operation are in such a strict coordination with each other. This type of the coordination is expected to be a symmetry-caused property. The explanation for this property is the following. The cone spiral structure of sublattice A [Eq. (11)] for arbitrary  $\mathbf{q}$  and  $\theta_A$  is invariant with respect to the SSG operation  $\{\Theta C_{2y}|I|0\}$  that combines space inversion  $I$  and spin transformation  $\Theta C_{2y}$  performing spin reflection in the  $xz$  plane. This operation leaves invariant also the cone structure of the sublattice B [Eq. (12)] but only in the case of  $\phi = 0$  or  $\phi = \pi$ . This means that if the calculation is started with  $\phi = 0$  the value of  $\phi$  remains zero during iterations since the symmetry with respect to the operation  $\{\Theta C_{2y}|I|0\}$  must be preserved. Thus, although there is no symmetry operation transforming the sublattices into each other there is an operation that is responsible for preserving  $\phi = 0$  and makes the two-sublattice magnetic configuration distinguished by an additional symmetry compared with the configurations obtained by a nonzero relative phase shift  $\phi$  between the sublattices. Hence, the choice of  $\phi = 0$  in the starting magnetic configuration imposes another symmetry constraint [25] in the magnon calculation that is additional to the constraint of generalized periodicity.

The presence of the symmetry operation effectively connecting inequivalent Mn sublattices influences also the properties of the Te atoms in the magnon states. In contrast to the Mn sublattices, the atoms of the two Te sublattices remain equivalent because the space inversion transforms the Te sublattices into each other. This operation influences also the directions of the induced Te moments since to keep this symmetry operation intact the induced atomic moments of the two Te sublattices must transform into each other. The straightforward symmetry analysis gives for the Te atoms in the unit cell

$$\theta_C = \theta_D \equiv \theta_{Te} \neq 0, \quad (13)$$

$$\phi_C + \phi_D = \mathbf{q} \mathbf{R}_{IC}, \quad (14)$$

where lattice vector  $\mathbf{R}_{IC} = \mathbf{a}_D - I\mathbf{a}_C$ . Although the values of angles  $\theta_C$ ,  $\theta_D$  and  $\phi_C$ ,  $\phi_D$  cannot be determined by symmetry arguments the knowledge of relations (13) and (14) allows to accelerate the convergence process for the magnon configurations by adequate preparation of the initial magnetic configurations. The calculation process includes the self-consistent determination of the directions of all atomic moments. This process can be rather time consuming. The knowledge of the symmetry relations between the moments of different atoms allows to decrease the number of the degrees of freedom and leads to a considerable reduction of the convergence time.

Here we give some further information concerning the calculated values of sublattice quantities entering Eqs. (11) and (12). The values of the Mn moments appeared to be very

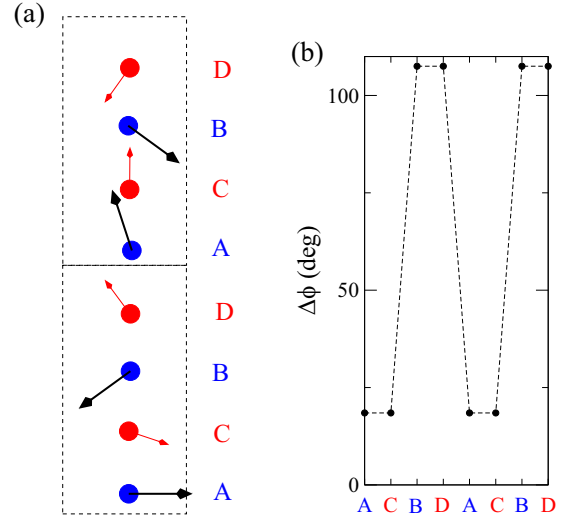


FIG. 8. (a) Directions of the projections of the atomic moments on the  $xy$  plane calculated for  $\mathbf{q} = (0,0,0.3)$  and  $\theta_A = 20^\circ$ . The atomic labeling is according to Fig. 2. Two unit cells adjacent along the  $z$  axis are presented. (b) For each atom, we show the value of the angle between the  $xy$  projection of its moment and of the moment of the atom lying next below.

robust and the difference between  $m_A$  and  $m_B$  was always small: for calculations with  $\theta_A = 20^\circ$ , it never exceeded a few thousandth of Bohr magniton for estimated Mn atomic moments of  $\sim 4.2\mu_B$ . On the other hand, the difference between  $\theta_A$  and  $\theta_B$  is an essential feature of the magnon states. It is strongly  $\mathbf{q}$ -dependent.

For field  $\mathbf{h}$  antiparallel to the  $z$  axis,  $\theta_A > \theta_B$ . Such magnon states have negative magnetization with respect to the  $z$  axis and is associated with sublattice A. For field  $\mathbf{h}$  parallel to the  $z$  axis  $\theta_A < \theta_B$ , the magnetization is positive, and magnon is associated with sublattice B. The magnons associated with different sublattices have opposite chiralities.

For completeness we give some results of the calculation of the values and directions of the induced Te moments. The both characteristics are  $\mathbf{q}$  dependent. The induced moments deviate rather weakly from the  $z = 0$  plane. For magnons of type A,  $\theta_{Te} > 90^\circ$  and the  $z$  component of the Te moments is negative. Respectively, for magnons of type B,  $\theta_{Te} < 90^\circ$  and the  $z$  component of the Te moments is positive. If the constrained deviation of the Mn moment is  $20^\circ$ , the maximal deviation of the Te moments from the  $z = 0$  plane is about  $20^\circ$ . The values of the induced moments in this case do not exceed a few thousandth of Bohr magniton. Therefore the contribution of the Te moments to the magnetization of the magnon states that is collinear to the  $z$  axis is weak. On the other hand, the contribution of the induced moments into magnon energy can be noticeable. For chirality degenerate magnons of A and B type, the values of the Te moments and of their deviations from the  $z = 0$  plane are exactly equal. For the chirality split magnons at a given  $\mathbf{q}$  the values are numerically different though in MnTe this difference is not large.

In Fig. 8(a), we show the directions of the projections of the moments on the  $xy$  plane calculated for  $\mathbf{q} = (0,0,0.3)$  and  $\theta_A = 20^\circ$ . Two unit cells adjacent along the  $z$  axis are

presented. The directions of the atomic moments in the second unit cell rotate by angle  $\mathbf{qR}$  with respect to the corresponding moments in the first unit cell. Here  $\mathbf{R}$  is the lattice vector connecting the cells. The relative directions of the Mn moments of sublattices A and B in the same unit cell are also according to wave vector  $\mathbf{q}$ :  $\phi_B - \phi_A = \mathbf{q}(\mathbf{a}_B - \mathbf{a}_A) + \pi$  that is the consequence of  $\phi = 0$  in Eq. (12). The directions of the Te moments (atoms C and D) within one unit cell cannot be uniquely determined by symmetry. There is, however, symmetry property of equal angles of the Te moments with respect to the moment of the Mn atom lying between them. On the other hand, these angles are different for the Mn atoms of the A and B sublattices reflecting their inequivalence in the magnon states. Figure 8(b) presents for each atom the value of the angle between the  $xy$  projection of its moment and of the moment of the atom lying next below. As seen in Fig. 8(a), this is always the angle between the moments of the Mn and Te atoms. These angles are distinctly different for Mn atoms of the A and B sublattices confirming again their inequivalence.

### E. Chirality splitting of magnons in altermagnets

To study the chirality properties of magnons the approach to the symmetry analysis must be fundamentally revised compared to the spin-splitting study of the electron states discussed above (Sec. IV B). Now the analysis is focused not on the properties of the electron states of the same magnetic configuration but on the relation between energies of different magnetic configurations. If we take an arbitrary SSG operation  $\{\alpha_S|\alpha_R|\tau\}$  and transform our magnetic system according Eq. (8), we obtain the system with the properties directly related to the properties of the initial system. This conservation of the properties reflects two factors: first, the homogeneity and anisotropy of the space where the system is placed and, second, the invariance under the applied transformation of the form of the interactions taken into account in the considered physical model [64]. In particular, the equivalence of the systems connected by the SSG transformation reflects the fact that both space shift and space rotation of the system does not change the energy of the system. To reveal the magnon states having, for symmetry reasons, equal energies we will act with operations  $\{\alpha_S|\alpha_R|\tau\}$  on a selected magnon state aiming to determine other magnon states equivalent to it. Since dealing with the magnon states of the system we are not interested in the copies of the system obtained by the displacement of the atomic lattice or by the rotation of the net sublattice magnetization from the  $z$  axis the operations we consider are restricted to follows: the orbital part  $[\alpha_R|\tau]$  of the transformation belongs to the space group of the crystal and leaves the lattice unchanged whereas the spin transformation  $\alpha_S$  keeps the net magnetizations of the sublattices collinear to the  $z$  axis.

If  $[\alpha_R|\tau]$  transforms magnetic sublattices into themselves the spin part must keep the directions of the sublattice magnetizations unchanged  $\alpha_S \mathbf{e}_z = \mathbf{e}_z$ . Here  $\mathbf{e}_z$  is the unity vector parallel to the  $z$  axis. Respectively, if  $[\alpha_R|\tau]$  transforms sublattices into each other the spin part must reverse the directions of the sublattice magnetizations  $\alpha_S \mathbf{e}_z = -\mathbf{e}_z$ . This shows that the set of the operations we need to consider forms exactly the SSG of the collinear AFM ground state that is the group

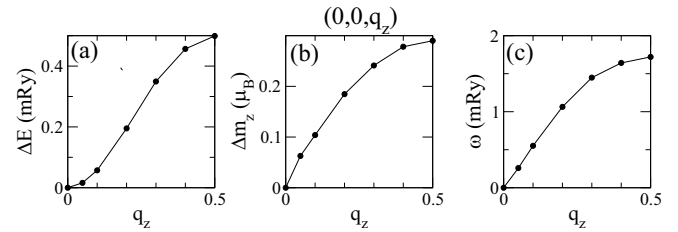


FIG. 9. Calculation of the spin wave energies in the  $\Gamma A$  interval of the BZ:  $\mathbf{q} = (0,0,q_z)$ ,  $q_z \in [0, 0.5]$ . (a)  $\Delta E$ , (b)  $\Delta m_z$ , (c) spin wave energy  $\omega$ .

used above (Sec. IV B) in the discussion of the altermagnetic spin splitting of the electronic states of the GS collinear configuration.

This conclusion reveals a direct analogy between the pattern of the spin splitting of the electron states in the  $\mathbf{k}$  space and the pattern of the chirality splitting of the spin waves in the  $\mathbf{q}$  space. Indeed, if  $\alpha_R$  transforms  $\mathbf{k}$  vector of an electron state in  $\alpha_R \mathbf{k}$  it transforms  $\mathbf{q}$  vector of a magnon in  $\alpha_R \mathbf{q}$ . And if this operation reverses spin of the electron state it changes also the chirality of the magnon. Hence if there is spin-splitting (spin-degeneracy) of the electron states at point  $\mathbf{k}$  there is also the chirality splitting (chirality degeneracy) of the magnon states for wave vector  $\mathbf{q} = \mathbf{k}$ . Therefore the reciprocal-space symmetry patterns of the spin splitting in the ground state electron band structure and chirality splitting of magnons are identical. In particular, Fig. 6 reflecting spin splitting of the electron states in the  $\mathbf{k}$  space is directly applicable to the analysis of the chirality splitting of the magnons in the  $\mathbf{q}$  space.

### F. Calculated magnon dispersion

In Fig. 9, we show the results of the calculation of the spin wave energies in the  $\Gamma A$  interval of the BZ:  $\mathbf{q} = (0,0,q_z)$ ,  $q_z \in [0, 0.5]$ . Close to the  $\Gamma$  point the energy increase  $\Delta E \sim q_z^2$  whereas  $\Delta m_z \sim q_z$ . This gives a linear dependence of the spin wave energy  $\omega$  on  $q_z$ , as expected for the magnons in AFMs in the region of the  $\Gamma$  point. In agreement with symmetry arguments, the magnons of both chiralities are degenerate at the wave vectors from this interval.

From the symmetry analysis (Sec. IV E), it is expected that for the wave vectors lying on a less symmetric line we should obtain chirality splitting of the magnon states. In Fig. 10, we

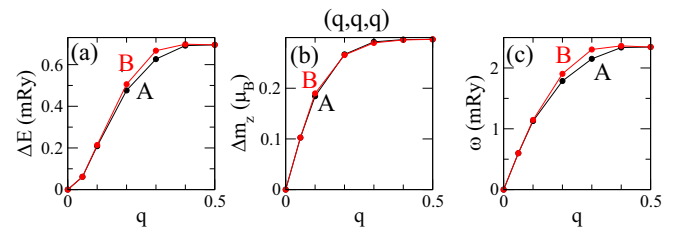


FIG. 10. Calculation of the spin wave energies in the interval  $\mathbf{q} = (q, q, q)$ ,  $q \in [0, 0.5]$ . (a)  $\Delta E$ , (b)  $\Delta m_z$ , (c) spin wave energy  $\omega$ . Black curves show the results for magnons of type A, red curves for magnons of type B.

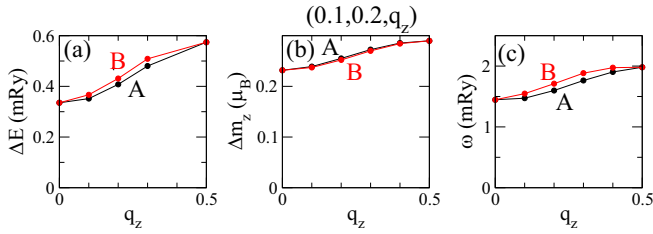


FIG. 11. Spin wave energies in the interval  $\mathbf{q} = (0.1, 0.2, q_z)$ ,  $q_z \in [0, 0.5]$ . (a)  $\Delta E$ , (b)  $\Delta m_z$ , (c) spin wave energy  $\omega$ . Black curves show the results for magnons of type A, red curves for magnons of type B.

show the result of the calculations for interval  $\mathbf{q} = (q, q, q)$ ,  $q \in [0, 0.5]$ . The calculations confirm the prediction of the symmetry analysis: numerical difference between data for A and B magnons is obtained for all points of the interval with exception for the end points. However, the difference is small and, for a part of the interval, is not noticeable in the figure.

In Fig. 11, we show the result of the calculations for an interval  $\mathbf{q} = (0.1, 0.2, q_z)$ ,  $q_z \in [0, 0.5]$  in the reciprocal space. This interval contains general points not invariant with respect to any symmetry operation. Again the calculations confirm the results of the symmetry analysis: at all inner points of the interval there is chirality splitting of the magnon states. The maximal splitting is  $\sim 7\%$  with respect to the energy of the spin waves at the corresponding  $\mathbf{q}$  point.

#### G. Instability of the energy of magnon state with respect to the number of magnons

While studying the performance of the method we carried out numerous model calculations. In particular, we investigated the consequences of the relative energy shift of the Mn 3d and Te 5p states that influences the hybridization between these states. Since the nonmagnetic atoms, in our case Te atoms, play crucial role in the formation of altermagnetism, the character of the hybridization of the electron states of magnetic and nonmagnetic atoms is an important factor influencing the character of the altermagnetic effects. As a convenient tool for varying the energy positions of the Mn 3d and Te 5p states we employed LDA +  $U$  method with various values of the corresponding  $U$  parameters. In these numerical experiments we used not only parameter  $U_{Mn}$  for the Mn 3d states but also small  $U_{Te}$  parameter for the Te 5p states, the latter treated as a free parameter assuming both positive and negative values. In these model calculations, we noticed that in some cases the spin wave states behave singular as the function of  $\Delta m_z$ .

In Fig. 12, we show a typical instability behavior. This result was obtained for the energy of the magnon states of type A with wave vector  $\mathbf{q} = (0.1, 0.2, 0.3)$  calculated as a function of constrained angle  $\theta_A$  with parameters  $U_{Mn} = 0.2$  Ry, and  $U_{Te} = -0.03$  Ry. The increase of  $\theta_A$  can be associated with increasing number of magnons. Around  $\theta_A$  of  $20^\circ$  the system experiences sharp transformation between two different states. It is straightforward to suppose that in this  $\theta_A$  region, the increase of  $\theta_A$  leads to the change of the relative energy positions of different groups of electron states in the band structure of the system. In the iterations, the conse-

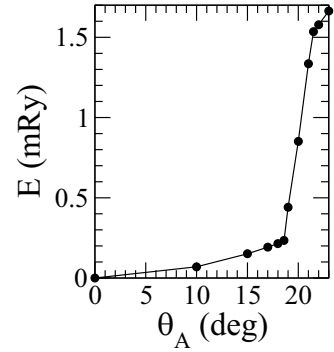


FIG. 12. Instability of the energy of magnon state with respect to the number of magnons.

quences of this process are enhanced leading to the sharp variation of the energy of the magnon state.

A similar unstable behavior we obtained for magnon B as a function of the constrained angle  $\theta_B$  (not shown). However, the region of instability was shifted to somewhat smaller angles. As the result, in the instability region we obtained an enhancement of the chirality splitting effect. Thus, for  $\theta_A = \theta_B = 20^\circ$ , the difference in energies of the A and B magnon states is  $\sim 0.6$  mRy that is about two orders of value larger than for angles of  $15^\circ$ . Similar instability was obtained in calculations for other wave vectors  $\mathbf{q}$ . The presence of such instabilities cannot be noticed applying the standard procedure of mapping on the Heisenberg Hamiltonian. The possibility to study such instabilities that are different for different magnon chirality channels is a useful feature of the suggested method.

#### H. Relation between electronic band structures of the magnon states and chirality properties of these states

Both chirality splitting and chirality degeneracy of two magnons manifest certain relation between the energies of the magnons. Whether two magnons are equivalent and have equal energies or are inequivalent and have different energies must be reflected in the properties of their electron band structures. In this section, we gain an insight into the connection between electronic band structures of the magnon states and chirality properties of these states. Our method includes the calculation of the electronic band structures of the magnons as a part of the iteration process.

The concepts of the generalized periodicity [Eq. (4)] and generalized Bloch theorem [39] will help us to establish the transformation path from the electronic band structure of the collinear AFM GS to the electronic band structure of the magnon with a given wave vector  $\mathbf{q}$  and given chirality. In this way, we reveal the features of the electron energy spectrum connected with the presence or absence of the chirality splitting.

We begin with the electron band structure of the ground state. As pointed out in Sec. IV B, the collinear magnetic ground state can be treated as a spiral with  $\theta = 0$  and arbitrary wave vector  $\mathbf{q}$ . Different  $\mathbf{q}$  values lead to different relative shifts of the spin-up and spin-down electron states in the reciprocal space. This shift is the consequence of the redefinition of the wave vector of the electron state in the

case of the generalized Bloch theorem compared to the usual periodicity and usual Bloch theorem [40]: depending on spin projection  $\sigma$  wave vector of the electron state changes from  $\mathbf{k}$  to  $\mathbf{k} - \sigma\mathbf{q}/2$ . Since in the collinear AFM GS there is no mixing between spin-up and spin-down electron states the relative shift of these states in the reciprocal space has no consequences for physically significant characteristics. However, in the noncollinear magnon state with  $\theta \neq 0$ , the wave vector  $\mathbf{q}$  is uniquely defined. The relative shift by vector  $\mathbf{q}$  of the spin-up and spin-down states is the first step in the transformation of the band structure that brings the wave vectors of the electron states in agreement with the definition according to the generalized Bloch theorem, the only possible way to introduce the wave vector in the case of noncollinear spiral structures.

The detailed process of the transformation of the shifted GS electronic band structure to the electronic band structure of the magnon in a real multiple-band system is complex and can be obtained only numerically. However, some important general trends can be distinguished. One of the consequences of the noncollinearity is the hybridization of the spin-up and spin-down electron states. The strongest hybridization takes place in the regions of the intersection of the spin-up and spin-down bands. From the symmetry point of view, in the collinear ground state the spin-up and spin-down electron states belong to different IRs of the SSG group and the corresponding bands intersect. In the magnon state, the number of the symmetry operations decreases and spin-up and spin-down states do not any longer belong to different IRs that leads to their hybridization. The hybridization leads to the repulsion of the bands at the intersection points.

We remark that besides the hybridization repulsion of the bands with opposite spin projections in the electron structure of the helical configuration the noncollinearity leads also to the transformation of the electron bands with a given spin projection that has the form of mixing of the  $\mathbf{k} - \mathbf{q}/2$  and  $\mathbf{k} + \mathbf{q}/2$  states of the GS electron structure with coefficients  $\cos^2 \frac{\theta}{2}$  and  $\sin^2 \frac{\theta}{2}$  (Ref. [39]). This effect is quadratic with respect to  $\theta$  while the spin-mixing effect at the intersection point is linear in  $\theta$ .

Since the positions of the band intersections are different for different  $\mathbf{q}$ , the process of the hybridization is  $\mathbf{q}$  dependent and, therefore, different for different magnons. Let us look closer at the transformation of the band structure for two values of the magnon wave vector  $\mathbf{q}$ : high-symmetry vector  $\mathbf{q}_1 = (0, 0, 0.2)$  and general vector  $\mathbf{q}_2 = (0.1, 0.2, 0.2)$ . On the basis of both the symmetry analysis and the calculations discussed in Secs. IV E and IV F, we know that at  $\mathbf{q}_1$  the magnons are chirality-degenerate whereas at  $\mathbf{q}_2$  they are chirality split. We begin with  $\mathbf{q}_1$  and consider electron band structure in the interval  $[0, 0, k_z]$ ,  $k_z \in [-0.5, 0.5]$ , in the  $\mathbf{k}$  space. On the high-symmetry line  $(0, 0, k_z)$  the GS band structure is spin degenerate [Fig. 7(a)]. The relative shift by  $\mathbf{q}_1$  results in spin split bands as shown in Fig. 13(a). The change of the sign of  $k_z$  combined with the spin reversal leaves the band structure in Fig. 13(a) invariant. The band structures of magnon configurations of both chiralities calculated for wave vector  $\mathbf{q}_1$  and  $(0, 0, k_z)$  line are presented in Figs. 13(b) and 13(c). For magnon configuration of type A, we used angles  $\theta_A = 45$  and  $\theta_B = 0$ , for magnon of type B angles  $\theta_A = 0$  and

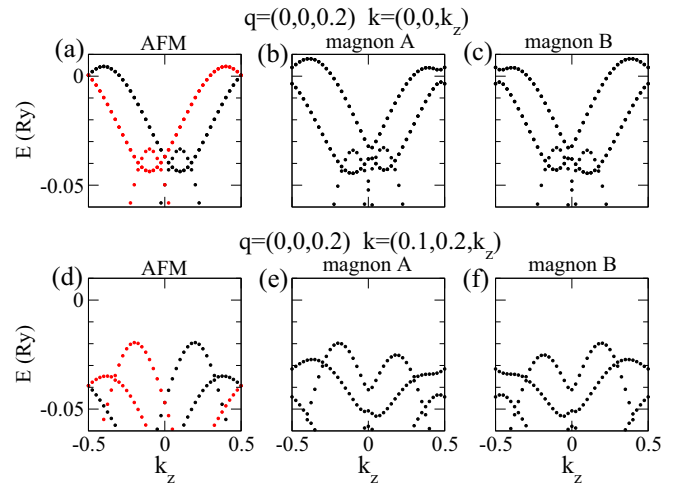


FIG. 13. The transformation of the electron band structure of the AFM GS to the band structure of magnon states with  $\mathbf{q}_1 = (0, 0, 0.2)$ . (a)–(c) present the bands in the interval  $[0, 0, k_z]$ ,  $k_z \in [-0.5, 0.5]$  of the electron BZ. The usual AFM band structure in this interval is shown in Fig. 7(a). (a) gives the AFM band structure after the shift of the bands by  $\frac{1}{2}\sigma\mathbf{q}_1$ . (b) and (c) give the electron bands for magnon structures of the A and B types. (d)–(f) give the band structure in the interval  $[0.1, 0.2, k_z]$ ,  $k_z \in [-0.5, 0.5]$ . Corresponding usual AFM band structure is shown in Fig. 7(b). (d) gives the AFM band structure after the shift of the bands by  $\frac{1}{2}\sigma\mathbf{q}_1$ . (e) and (f) give the electron bands for magnon structures of the A and B types. In (a) and (d), black (red) circles present spin-up (spin-down) states.

$\theta_B = 45$ . Since in noncollinear structures, the electron states are spin-mixed, all states are shown in the same color. The band structures of magnons A and B are different and both of them have lost the symmetry with respect to the reflection at  $k_z = 0$ . However, these band structures transform to each other after reflection at  $k_z = 0$  and, therefore, the integrals over the occupied parts of the spectra for the given  $\mathbf{k}$  interval are equal for both magnons.

Let us continue with the consideration of a low-symmetry interval  $[0.1, 0.2, k_z]$ ,  $k_z \in [-0.5, 0.5]$ . The bands have alternating spin splitting in the collinear AFM configuration [Fig. 7(b)]. There is the symmetry of the band structure with respect to simultaneous sign change of both  $k_z$  and spin projection similar to the case shown in Fig. 13(a). After the shift by  $\frac{1}{2}\sigma\mathbf{q}_1$  [Fig. 13(d)], the symmetry between the spin-up and spin-down bands remains intact. The calculation for the A and B magnon configurations for this  $\mathbf{q}$  gives, similar to the  $(0, 0, k_z)$  interval, two different band structures [Figs. 13(e) and 13(f)] which have lost the reflection symmetry. However, they again transform into each other after reflection at  $k_z = 0$ . Therefore, also in this case, the integrals over occupied parts of the band structures of both magnons are identical. These symmetry properties provide an insight into why the magnons with opposite chiralities are degenerate at  $\mathbf{q}_1 = (0, 0, 0.2)$ . Now let us consider the magnons with low-symmetry wave vector  $\mathbf{q}_2 = (0.1, 0.2, 0.3)$  that is not invariant with respect to any space group transformation. We take again the  $[0.1, 0.2, k_z]$  interval of the BZ. After  $\frac{1}{2}\sigma\mathbf{q}_2$  shift in the GS band structure [Fig. 14(a)], we obtain in this interval the spin-up and spin-down bands that are essentially



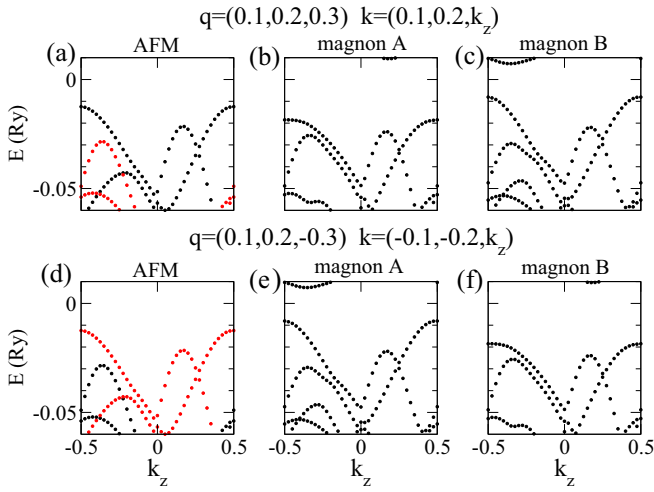


FIG. 14. The transformation of the electron band structure of the AFM GS to the band structures of magnon states with wave vectors  $\mathbf{q}_2 = (0.1, 0.2, 0.3)$  and  $\mathbf{q}_3 = (0.1, 0.2, -0.3)$ . (a)–(c) give the band structures in the interval  $[0.1, 0.2, k_z]$ ,  $k_z \in [-0.5, 0.5]$  of the electron BZ for wave vector  $\mathbf{q}_2$ . (a) presents the AFM bands after the shift by  $\frac{1}{2}\sigma\mathbf{q}_2$ . (b) and (c) give the electron bands for magnon structures of the A and B type. (d)–(f) show the band structures in the interval  $[-0.1, -0.2, k_z]$ ,  $k_z \in [-0.5, 0.5]$  for wave vector  $\mathbf{q}_3$ . (d) gives the AFM bands after the shift by  $\frac{1}{2}\sigma\mathbf{q}_3$ . (e) and (f) give the electron bands for magnon structures of the A and B type. In (a) and (d), black (red) circles present spin-up (spin-down) states.

different and cannot be transformed into each other by a symmetry operation. Respectively, magnons A and B result in this case in two essentially different band structures [Figs. 14(b) and 14(c)] giving different energy contributions to the integral band energies of the A and B magnons. The difference of the band structures of the A and B magnons with wave vector  $\mathbf{q}_2$  illustrates the origin of the chirality splitting of the magnons at this wave vector.

On the other hand, for  $\mathbf{q}_3 = (0.1, 0.2, -0.3)$  in the  $[-0.1, -0.2, k_z]$  interval we obtain the band structures [Figs. 14(d)–14(f)] very similar to those shown in Figs. 14(a)–14(c). Figure 14(d) for the AFM GS is identical to Fig. 14(a) after reversal of the spin projections of all electron states. The band structure of magnon A with wave vector  $\mathbf{q}_3$  [Fig. 14(e)] is identical to the band structure of magnon B with wave vector  $\mathbf{q}_2$  [Fig. 14(c)]. The band structure of magnon B with wave vector  $\mathbf{q}_3$  [Fig. 14(f)] is identical to the band structure of magnon A with wave vector  $\mathbf{q}_2$  [Fig. 14(b)]. These properties of the band structures illustrate the band-structure basis of the chirality degeneracy of the magnons with different wave vectors and chirality splitting at given wave vectors.

The following point is worth emphasizing: As noted above, in the band structures of magnons (Figs. 13 and 14) the electron states are spin mixed and, therefore, all bands are presented in the same color. However, the contributions of the spin-up and spin-down components of the spinor eigenfunctions are different for different states. Some of the electron states can remain almost spin-up or almost spin-down. On the other hand, in the regions where spin-up and spin-down bands intersect in the GS the hybridization

leads to the electron states with large contributions of both spin projections. For magnons, the integrated spin contributions of the occupied electron states do not completely compensate each other since each magnon has a nonzero magnetic moment.

## V. CONCLUSIONS

In the paper, we suggest the method for direct *ab initio* calculation of magnons in complex collinear magnets without the spin-orbit coupling. The method does not include the mapping of the electron system on the Heisenberg Hamiltonian of the interacting atomic moments as an intermediate step.

Each magnon state is obtained in a separate DFT based self-consistent calculation performed under two different constraints. One constraint governs the magnetization change with respect to the ground state and the other is a symmetry constraint establishing the value of the magnon wave vector  $\mathbf{q}$ . The performance of the method is demonstrated by the application to an altermagnet MnTe. The main feature of the GS of the altermagnets is the spin splitting of the electron states with a given wave vector  $\mathbf{k}$ . Also the magnons in altermagnets have a special feature: chirality splitting of magnons with the same wave vector  $\mathbf{q}$  that is the energy difference of the magnons corresponding to the different magnetic sublattices. We show that despite different nature of the spin-splitting of the electron states and chirality splitting of the magnon states have identical patterns in the corresponding wave vector spaces. All conclusions based on the symmetry arguments are confirmed by the results of numerical calculations.

Our method allows investigation of the electron band structure of individual magnons. We investigate the connection between the chirality properties of the magnons and the properties of the electron band structures of the magnons. The deep connection between these two different energy characteristics is exposed.

The altermagnetism of MnTe is the consequence of the presence of the Te atoms. The method allows the study of the self-consistent response of the nonmagnetic atoms to the formation of magnon excitations. An adequate attention is devoted to the analysis of the properties of the Te atoms in magnons in MnTe. In particular, we show that the Te atoms remain equivalent in the magnon states though the Mn atoms belonging to different sublattices became inequivalent. The information about induced magnetic moments of the Te atoms obtained in the symmetry analysis besides providing important physical information helps to accelerate the numerical convergence of the magnon states by means of decreasing the number of degrees of freedom in the self-consistent calculations.

In the paper, different symmetry aspects are analyzed within the framework of the spin space groups. These aspects include the symmetry constraint of generalized periodicity in the suggested method of the magnon calculations, the spin splitting of the electron states in the GS, and chirality splitting of the magnon states. The SSGs that are the generalization of the usual space groups allow the integration of these different aspects in one coherent physical picture.

The suggested method accompanied with symmetry arguments on the basis of the spin-space groups provides a new

tool making possible efficient direct first principles study of the magnons in complex collinear magnets including emerging class of altermagnets.

The spin splitting in some of the AFM crystals was known for many years but only few years ago it became the focus of intense research efforts within the new research field dubbed altermagnetism. Possible applications of the altermagnetic spin splitting are under discussion. On the other hand, the chiral splitting of the magnon states that is a fundamental feature of altermagnets has been noticed very recently. Though important from the theoretical point of view, this splitting seems to be relatively weak. However, also this feature of altermagnets can become important for future experimental studies and practical applications in the field of magnonics. A necessary step on this path is the search for materials with large chirality splitting. Our method that self-consistently takes into account the crucial contribution of the nonmagnetic atoms provides a useful tool in this search. Also, the ability of the method to reveal possible chirality-sensitive instabilities of the magnon excitations can prove itself useful in this respect.

An important question is if the method can be applied to the systems where the SOC cannot be neglected. The main problem with the SOC is that it reduces the 6D space with separate spin and orbital variables to the actual 3D space where any point transformation acts on both types of variables. In the presence of SOC, the generalized translations do not commute with the Kohn-Sham Hamiltonian and the reduction of the problem, for an arbitrary wave vector  $\mathbf{q}$ , to the small crystallographic unit cell cannot be performed. This mathematical problem is the reflection of the physical reality consisting in the fact that the SOC disturbs the perfect helical structure of the spin waves by means of the magnetic anisotropy. However, there is an important class of

materials where the method can potentially be applied in the presence of the SOC. These are the materials with uniaxial magnetic anisotropy. If the  $z$  axis is an easy axis and the anisotropy in the  $xy$  plane is negligible, the spin rotation by an arbitrary angle about the anisotropy axis leaves the system invariant, and the generalized translation symmetry remains intact. In Ref. [65], the possibility to neglect the in-plane anisotropy was used to study the Dzyaloshinskii-Moriya interaction that is one of the consequences of SOC. The extension of the direct method suggested in this paper to the case of the magnets with uniaxial anisotropy is an interesting problem for the future studies. Another possibility to deal with the SOC is, first, to perform self-consistent calculation of the magnon states without SOC and then to take into account the SOC within the first-order perturbation theory [66].

## ACKNOWLEDGMENTS

The discussions with Samir Lounis are gratefully acknowledged. K.C. acknowledges financial support by Czech Science Foundation, Grant No. 23-04746S, and project Quantum materials for applications in sustainable technologies (QM4ST), funded as Project No. CZ.02.01.01/00/22\_008/0004572 by P JAK, Ministry of Education, Youth and Sports of the Czech Republic. V.M.S. acknowledges financial support by Grant No. PID2022-139230NB-I00 funded by MCIN/AEI/10.13039/501100011033.

## DATA AVAILABILITY

The data that support the findings of this article are not publicly available. The data are available from the authors upon reasonable request.

- 
- [1] B. Flebus *et al.*, The 2024 magnonics roadmap, *J. Phys.: Condens. Matter* **36**, 363501 (2024).
  - [2] A. V. Chumak *et al.*, Advances in magnetics roadmap on spin-wave computing, *IEEE Trans. Magn.* **58**, 1 (2022).
  - [3] A. Barman *et al.*, The 2021 magnonics roadmap, *J. Phys.: Condens. Matter* **33**, 413001 (2021).
  - [4] H. J. Qin, K. Zakeri, A. Ernst, L. M. Sandratskii, P. Buczek, A. Marmodoro, T.-H. Chuang, Y. Zhang, and J. Kirschner, Long-living terahertz magnons in ultrathin metallic ferromagnets, *Nat. Commun.* **6**, 6126 (2015).
  - [5] C. Kittel, *Introduction to Solid State Physics* (Wiley, Hoboken, New Jersey, 2004).
  - [6] S. V. Halilov, H. Eschrig, A. Y. Perlov, and P. M. Oppeneer, Adiabatic spin dynamics from spin-density-functional theory: Application to Fe, Co, and Ni, *Phys. Rev. B* **58**, 293 (1998).
  - [7] Q. Niu, Xindong Wang, L. Kleinman, and W.-M. Liu, D. M. C. Nicholson, and G. M. Stocks, Adiabatic dynamics of local spin moments in itinerant magnets, *Phys. Rev. Lett.* **83**, 207 (1999).
  - [8] S. Y. Savrasov, Linear response calculations of spin fluctuations, *Phys. Rev. Lett.* **81**, 2570 (1998).
  - [9] P. Buczek, A. Ernst, and L. M. Sandratskii, Different dimensionality trends in the Landau damping of magnons in iron, cobalt, and nickel: Time-dependent density functional study, *Phys. Rev. B* **84**, 174418 (2011).
  - [10] L. M. Sandratskii and P. Buczek, Lifetimes and chirality of spin waves in antiferromagnetic and ferromagnetic FeRh from the perspective of time-dependent density functional theory, *Phys. Rev. B* **85**, 020406(R) (2012).
  - [11] M. M. Odashima, A. Marmodoro, P. Buczek, A. Ernst, and L. Sandratskii, Chirality-dependent magnon lifetime in a compensated half-metallic ferrimagnet, *Phys. Rev. B* **87**, 174420 (2013).
  - [12] S. Lounis, M. D. S. Dias, and B. Schweefinghaus, Transverse dynamical magnetic susceptibilities from regular static density functional theory: Evaluation of damping and  $g$  shifts of spin excitations, *Phys. Rev. B* **91**, 104420 (2015).
  - [13] T. Skovhus and T. Olsen, Dynamic transverse magnetic susceptibility in the projector augmented-wave method: Application to Fe, Ni, and Co, *Phys. Rev. B* **103**, 245110 (2021).
  - [14] X. Liu, L. Yihao, and J. Feng, Implementation of the density functional perturbation theory for generalized susceptibility in the projector augmented wave framework, *Phys. Rev. B* **108**, 094405 (2023).
  - [15] A. I. Liechtenstein, M. I. Katsnelson, V. P. Antropov, and V. A. Gubanov, Local spin density functional approach to the theory of exchange interactions in ferromagnetic metals and alloys, *J. Magn. Magn. Mater.* **67**, 65 (1987).

- [16] S. Mankovsky and H. Ebert, First-principles calculation of the parameters used by atomistic magnetic simulations, *Electron. Struct.* **4**, 034004 (2022).
- [17] I. Turek, J. Kudrnovský, V. Drchal, and P. Bruno, Exchange interactions, spin waves, and transition temperatures in itinerant magnets, *Philos. Mag.* **86**, 1713 (2006).
- [18] S. Mu, R. P. Hermann, S. Gorsse, H. Zhao, M. E. Manley, R. S. Fishman, and L. Lindsay, Phonons, magnons, and lattice thermal transport in antiferromagnetic semiconductor MnTe, *Phys. Rev. Mater.* **3**, 025403 (2019).
- [19] G. Martínez-Carracedo, L. Oroszlany, A. Garcia-Fuente, B. Nyari, L. Udvardi, L. Szunyogh, and J. Ferrer, Relativistic magnetic interactions from nonorthogonal basis sets, *Phys. Rev. B* **108**, 214418 (2023).
- [20] M. Ležaić, P. Mavropoulos, J. Enkovaara, G. Bihlmayer, and S. Blügel, Thermal collapse of spin polarization in half-metallic ferromagnets, *Phys. Rev. Lett.* **97**, 026404 (2006).
- [21] L. M. Sandratskii, R. Singer, and E. Sasioglu, Heisenberg Hamiltonian description of multiple-sublattice itinerant-electron systems: General considerations and applications to NiMnSb and MnAs, *Phys. Rev. B* **76**, 184406 (2007).
- [22] J. Sodequist and T. Olsen, Two-dimensional altermagnets from high throughput computational screening: Symmetry requirements, chiral magnons, and spin-orbit effects, *Appl. Phys. Lett.* **124**, 182409 (2024).
- [23] A. Szilva, Y. Kvashnin, E. A. Stepanov, L. Nordström, O. Eriksson, A. I. Lichtenstein, and M. I. Katsnelson, Quantitative theory of magnetic interactions in solids, *Rev. Mod. Phys.* **95**, 035004 (2023).
- [24] We remark that the contribution of Ref. [7] was to show that Eq. (1), although expected from the general concept of spin waves can be derived in the DFT context. In this respect, Ref. [7] contributes to the theoretical fundament of our method. However, the mathematical apparatus of Berry curvatures used in Ref. [7] does not provide a basis for a practical method for a direct DFT-study of magnons in complex materials. To suggest such a method is one of the tasks of this paper.
- [25] L. M. Sandratskii, Magnetic structure of relativistic systems with low symmetry, *Phys. Rev. B* **64**, 134402 (2001).
- [26] L. Šmejkal, J. Sinova, and T. Jungwirth, Beyond conventional ferromagnetism and antiferromagnetism: A phase with nonrelativistic spin and crystal rotation symmetry, *Phys. Rev. X* **12**, 031042 (2022).
- [27] L. Šmejkal, J. Sinova, and T. Jungwirth, Emerging research landscape of altermagnetism, *Phys. Rev. X* **12**, 040501 (2022).
- [28] I. Mazin, Editorial: Altermagnetism—a new punch line of fundamental magnetism, *Phys. Rev. X* **12**, 040002 (2022).
- [29] L. Bai, W. Feng, S. Liu, L. Šmejkal, Y. Mokrousov, and Y. Yao, Altermagnetism: Exploring new frontiers in magnetism and spintronics, *Adv. Funct. Mater.* **34**, 2409327 (2024).
- [30] S. Reimers *et al.*, Direct observation of altermagnetic band splitting in CrSb thin films, *Nat. Commun.* **15**, 2116 (2024).
- [31] J. Krempaský *et al.*, Altermagnetic lifting of Kramers spin degeneracy, *Nature (London)* **626**, 517 (2024).
- [32] I. I. Mazin, Altermagnetism in MnTe: Origin, predicted manifestations, and routes to detwinning, *Phys. Rev. B* **107**, L100418 (2023).
- [33] O. Fedchenko *et al.*, Observation of time-reversal symmetry breaking in the band structure of altermagnetic RuO<sub>2</sub>, *Sci. Adv.* **10**, ead4883 (2024).
- [34] L. Šmejkal, A. Marmodoro, K.-H. Ahn, R. González-Hernández, I. Turek, S. Mankovsky, H. Ebert, S. W. D'Souza, O. Šipr, J. Sinova, and T. Jungwirth, Chiral magnons in altermagnetic RuO<sub>2</sub>, *Phys. Rev. Lett.* **131**, 256703 (2023).
- [35] Z. Liu, M. Ozeki, S. Asai, S. Itoh, and T. Masuda, Chiral split magnon in altermagnetic MnTe, *Phys. Rev. Lett.* **133**, 156702 (2024).
- [36] M. Alaei, P. Sobieszczyk, A. Ptok, N. Rezaei, A. R. Oganov, and A. Qaiumzadeh, Origin of A-type antiferromagnetism and chiral split magnons in altermagnetic  $\alpha$ -MnTe, *Phys. Rev. B* **111**, 104416 (2025).
- [37] S. M. Rezende, A. Azevedo, and R. L. Rodríguez-Suárez, Introduction to antiferromagnetic magnons, *J. Appl. Phys.* **126**, 151101 (2019).
- [38] L. M. Sandratskii, Noncollinear magnetism in itinerant-electron systems: Theory and applications, *Adv. Phys.* **47**, 91 (1998).
- [39] L. M. Sandratskii, Energy band structure calculations for crystals with spiral magnetic structure, *Physica Status Solidi (b)* **136**, 167 (1986).
- [40] L. M. Sandratskii, Symmetry analysis of electronic states for crystals with spiral magnetic order. I. General properties, *J. Phys.: Condens. Matter* **3**, 8565 (1991).
- [41] A. R. Williams, J. Kübler, and C. D. Gelatt, Cohesive properties of metallic compounds: Augmented-spherical-wave calculations, *Phys. Rev. B* **19**, 6094 (1979).
- [42] V. Eyert, *The Augmented Spherical Wave Method*, Lecture Notes in Physics Vol. 849 (Springer-Verlag, Berlin, Heidelberg, 2013).
- [43] U. von Barth and L. Hedin, A local exchange-correlation potential for the spin polarized case, *J. Phys. C* **5**, 1629 (1972).
- [44] M. Uhl, L. M. Sandratskii, and J. Kübler, Electronic and magnetic states of  $\gamma$ -Fe, *J. Magn. Magn. Mater.* **103**, 314 (1992).
- [45] A. Miyake, L. M. Sandratskii, A. Nakamura, F. Honda, Y. Shimizu, D. Li, Y. Homma, M. Tokunaga, and D. Aoki, Magnetic field effect on the chiral magnetism of noncentrosymmetric UPTGe: Experiment and theory, *Phys. Rev. B* **98**, 174436 (2018).
- [46] S. L. Dudarev, G. A. Botton, S. Y. Savrasov, C. J. Humphreys, and A. P. Sutton, Electron-energy-loss spectra and the structural stability of nickel oxide: An LSDA+U study, *Phys. Rev. B* **57**, 1505 (1998).
- [47] A. V. Shubnikov and N. V. Belov, *Colored Symmetry* (Pergamon Press, Oxford, 1964).
- [48] H. Padmanabhan, J. M. Munro, I. Dabo, and V. Gopalan, Antisymmetry: Fundamentals and applications, *Annu. Rev. Mater. Res.* **50**, 255 (2020).
- [49] W. F. Brinkman and R. J. Elliott, Theory of spin-space groups, *Proc. R. Soc. London, Ser. A* **294**, 343 (1966).
- [50] W. Brinkman and R. J. Elliott, Space group theory for spin waves, *J. Appl. Phys.* **37**, 1457 (1966).
- [51] A. P. Cracknell, Group theory in solid-state physics is not dead yet alias some recent developments in the use of group theory in solid-state physics, *Adv. Phys.* **23**, 673 (1974).
- [52] A. Corticelli, R. Moessner, and P. A. McClarty, Spin-space groups and magnon band topology, *Phys. Rev. B* **105**, 064430 (2022).
- [53] Z. Xiao, J. Zhao, Y. Li, R. Shindou, and Z.-D. Song, Spin space groups: Full classification and applications, *Phys. Rev. X* **14**, 031037 (2024).

- [54] X. Chen, J. Ren, Y. Zhu, Y. Yu, A. Zhang, P. Liu, J. Li, Y. Liu, C. Li, and Q. Liu, Enumeration and representation theory of spin space groups, *Phys. Rev. X* **14**, 031038 (2024).
- [55] Y. Jiang, Z. Song, T. Zhu, Z. Fang, H. Weng, Z.-X. Liu, J. Yang, and C. Fang, Enumeration of spin-space groups: Toward a complete description of symmetries of magnetic orders, *Phys. Rev. X* **14**, 031039 (2024).
- [56] W. Szuszkiewicz, E. Dynowska, B. Witkowska, and B. Hennion, Spin-wave measurements on hexagonal MnTe of NiAs-type structure by inelastic neutron scattering, *Phys. Rev. B* **73**, 104403 (2006).
- [57] S. Wakoh and J. Yamashita, Band structure of ferromagnetic iron self-consistent procedure, *J. Phys. Soc. Jpn.* **21**, 1712 (1966).
- [58] S. Asano and J. Yamashita, Band theory of antiferromagnetic chromium, *J. Phys. Soc. Jpn.* **23**, 714 (1967).
- [59] To remind, if  $\alpha_R \mathbf{k} = \mathbf{k} + \mathbf{K}_\mu$  where  $\mathbf{K}_\mu$  is reciprocal lattice vector, it is considered as identical to  $\mathbf{k}$  and is not included in  $\{\mathbf{k}\}$ .
- [60] L. M. Sandratskii, R. F. Egorov, and A. A. Berdyshev, Energy band structure and electronic properties of NiAs type compounds. II. Antiferromagnetic manganese telluride, *Physica Status Solidi (b)* **104**, 103 (1981).
- [61] I. Turek, Altermagnetism and magnetic groups with pseudoscalar electron spin, *Phys. Rev. B* **106**, 094432 (2022).
- [62] L. M. Sandratskii, Classification of single-electron states in a crystal on the basis of spin space groups, *Sov. Phys. J.* **22**, 941 (1979).
- [63] The direction of the field  $\mathbf{h}$  is opposite for the magnons of the A and B types.
- [64] The formula of the SOC is not invariant with respect to the  $\{\alpha_S|\alpha_R|\tau\}$  operations with different  $\alpha_S$  and  $\alpha_R$ . Therefore in the relativistic case the new system obtained by transformation  $\{\alpha_S|\alpha_R|\tau\}$  is essentially different from the initial one.
- [65] L. M. Sandratskii, Insight into the Dzyaloshinskii-Moriya interaction through first-principles study of chiral magnetic structures, *Phys. Rev. B* **96**, 024450 (2017).
- [66] M. Heide, G. Bihlmayer, and S. Blügel, Describing Dzyaloshinskii–Moriya spirals from first principles, *Phys. B: Condens. Matter* **404**, 2678 (2009).